Design Exploration of a Distributed Electric Propulsion Aircraft Using Explainable Surrogate Models

Pramudita Satria Palar, Eric Nguyen Van, Nathalie Bartoli, Joseph Morlier

Design Exploration of a Distributed Electric Propulsion Aircraft using Explainable Surrogate Models

Pramudita Satria Palar*
Bandung Institute of Technology, Bandung, West Java, 40132, Indonesia

Eric Nguyen Van †, Nathalie Bartoli ‡
DTIS, ONERA, Université de Toulouse, 3100 Toulouse, France
Fédération ENAC ISAE-SUPAERO ONERA, Université de Toulouse, 31000, Toulouse, France

Joseph Morlier§
ICA, Université de Toulouse, ISAE-SUPAERO, MINES ALBI, UPS, INSA, CNRS, 3 rue Caroline Aigle, Toulouse, 31400, France

Distributed electric propulsion in aircraft design is a concept that involves placing multiple electric motors across the aircraft's airframe. Such a system has the potential to contribute to sustainable aviation by significantly reducing greenhouse gas emissions, minimizing noise pollution, improving fuel efficiency, and encouraging the use of cleaner energy sources. This paper investigates the impact and relationship of turbo-electric propulsion component characteristics with three performance quantities of interest: lift-to-drag ratio, operating empty weight, and fuel burn. Using the small and medium-range "DRAGON" aircraft concept, we performed design exploration enabled through the explainable surrogate model strategy. This work uses Shapley Additive Explanations (SHAP) to illuminate the dependencies of these critical performance metrics on specific turbo-electric propulsion component characteristics, offering valuable insights to inform future advancements in electric propulsion technology. Through global sensitivity analysis, the study reveals a significant impact of electrical power unit (EPU) power density on lift-to-drag ratio, alongside notable roles played by EPU-specific power and applied voltage. For operating empty weight, EPU-specific power and voltage are highlighted as critical factors, while turboshaft power-specific fuel consumption notably influences fuel burn. The analysis concludes by exploring the implications of the insights for the future development of turbo-electric propulsion technology.

*Corresponding author, Assistant Professor, Faculty of Mechanical and Aerospace Engineering, email: pramsp@itb.ac.id.
†Researcher, email: eric.nguyen_van@onera.fr
‡Senior Researcher, email: nathalie.bartoli@onera.fr
§Professor, email: joseph.morlier@isae-supaero.fr

I. Introduction

Distributed Electric Propulsion (DEP) for aircraft refers to the distribution of thrust generation electrical devices such that mutual interactions between aerodynamics, propulsion and structure improve the overall efficiency of the aircraft. In most DEP concepts for commercial aviation, a gas turbine generator is used for electrical power generation. A redundant transmission system then routes the electrical power to the electric motors. Some concepts use DEP for drag reduction through boundary layer ingestion with Blended Wing Body aircraft ([1] and [2]) or on the fuselage ([3]), whereas other concepts use DEP to increase propulsive efficiency ([4], [5]). Such a new propulsion concept is studied at a preliminary stage using a multi-disciplinary design process and simple models to explore the design space quickly.

One objective of this paper is to analyze the impact of turbo-electric component characteristics on the propulsive performance of a DEP aircraft. The knowledge obtained from such endeavour will be particularly useful for further development of electric components to understand the technological performance requirements for successful applications. Usually, a global sensitivity analysis (GSA) is used to identify the most impacting variables, and optimization methods can be used to quickly explore and locate the best region of the design space [6, 7]. Difficulties can arise when the complexity of the design process increases with a growing number of design variables and interactions between disciplines, as is the case for DEP. In such cases, design exploration can become expensive, and a surrogate model may be used to reduce the exploration time.

Surrogate models are utilized to assist in deducing the design guideline. A surrogate model is an approximation model that yields fast-to-evaluate prediction useful for design exploration. In this paper, the surrogate model captures the relationship between the turbo-electric component characteristics with three quantities of interest (QOIs), namely, lift-to-drag ratio (L/D), operating empty weight (OEW), and fuel burn. The input parameters correspond to the characteristics of the electrical power unit (EPU), power generation, and power transmission, with a total of eight variables. However, it is difficult to infer important design insight from a surrogate model due to its black-box nature. To that end, we utilize the framework of an explainable surrogate model by extracting the dependency of the QOIs on each input variable. The concept of explainability, emerging from the machine learning domain, pertains to the capacity of the model to offer clear and interpretable explanations for its predictions, aiming to uncover insights from a surrogate or machine learning model that might otherwise be challenging to interpret due to its black-box nature [8]. That is, a surrogate model should not be perceived solely as a tool for making predictions; rather, it should also be seen as a means to acquire physical or design insights [9]. The framework combines an interpolation/regression model with explainability techniques to “dissect" a surrogate to understand the input-output relationship better. In this paper, we coupled the polynomial chaos expansion (PCE) [10] surrogate model with Shapley additive explanations (SHAP) [11] and used them for analyzing the turbo-electric component characteristics. SHAP is an explainability technique originating from machine learning and game theory, which decomposes a black-box function’s prediction into the individual contribution of each input by considering how much each input contributes to the prediction compared to its absence. SHAP offers

the advantage of unifying various previous explainability methods, including partial dependence plots [12], individual conditional expectations [13], locally interpretable model-agnostic explanations [14], and Shapley sampling values [15].

PCE was opted as a surrogate model due to its high accuracy for the problem considered in this paper. Besides, the analytical technique to extract SHAP values from PCE is available [16], which enables swift computation of the SHAP values. Most importantly, SHAP enables visualization of the function's inner workings and presents design insight. A few instances of how SHAP is applied in aerospace engineering include its use in understanding the influence of shape deformation on aerodynamic design optimization [17] and assessing the strength of composite laminates following multiple impacts [18]. Moreover, there is a growing interest in using SHAP to gain insights into constitutive modelling, particularly in turbulence modelling within the framework of the Reynolds-Averaged Navier Stokes (RANS) solver [19, 20]. In the context of this paper, SHAP enables easy and intuitive knowledge discovery of the relationship between the turbo-electric component characteristics and the aircraft performance, which is essential for future design endeavours. The Sobol indices [21], which can be analytically extracted for a PCE model [22], are also used in conjunction with the averaged SHAP for GSA to assess the importance of each input from a different viewpoint.

The main objective of this paper is to analyze the impact of turbo-electric component characteristics on the overall performance of a DEP aircraft. The knowledge obtained from such endeavour will be particularly useful for the further development of electric components. Section II defines the DEP concept and its characteristics to address this objective. Section III describes the surrogate models based on PCE and Shapley techniques. Results on the DEP concept are provided in Section IV with different plot analyses and coefficient tables to explain the behaviour. Conclusions and perspectives are drawn in Section V.

II. Problem definition

A. DRAGON configuration

The current study employs the "DRAGON" aircraft concept (see Fig. 1) as the baseline for investigating the characteristics of turbo-electric components on performance. The concept was introduced to investigate the potential adoption of a hybrid electric distributed propulsion system on a 150-passenger transport aircraft, operating at a cruise Mach number of 0.78 and covering a distance of 2750 NM [23–25].

The idea behind the DRAGON concept is to take advantage of DEP to maximize propulsive efficiency. One possibility to do so is by increasing the amount of air being accelerated by the fan or the so-called By-Pass Ratio (BPR). On traditional turbofan engines, this calls for an ever larger fan, to the point where the integration of the turbofan on the aircraft is becoming problematic (increased nacelle drag, insufficient ground clearance, higher mass, centre of gravity shift, etc). The idea for DRAGON is to replace a large turbofan with many small electric fans positioned at the wing trailing edge and powered by a gas turbine generator. Such a configuration allows to reach BPR of the order of 40

Fig. 1 The DRAGON aircraft concept

compared to 11 for the current state-of-the-art [26]. A very high propulsive efficiency can be achieved, although it comes at the cost of additional power transmission losses, added propulsion weight and additional aerodynamic interactions. To evaluate the overall impact of turbo-electric propulsion, the aircraft is studied in a multi-disciplinary analysis framework called FAST-OAD [27]. It is based on a combination of low-fidelity and semi-empirical models. The design process is illustrated in Fig. 2 with six components considered and the number of coupling variables involved.

The aircraft is sized based on Top Level Requirements such as the number of passengers and the range. The first component *geometry* computes the size of the fuselage and wing based on the number of passengers and an initial weight estimation. The component *propulsion_hep* calculates the nominal power of all the propulsive components according to thrust and power requirements evaluated during the mission evaluation. The *weight* component then computes the weight of the airframe and the propulsion system. The tail and wing surface area are updated in the component *tail_sizing* and after evaluation of the aerodynamics performance the fuel consumption is evaluated by time simulation in the component *performance*. The process loops over the take-off weight until convergence.

As turbo-electric propulsion is a new topic for commercial aviation, the evaluation of electric component performance is subject to uncertainty. Even more so are the technological improvements one can expect in the horizon of 2035 or 2050. In this context, the IMOTHEP project [28] was initiated to significantly improve hybrid-electric propulsion performance prediction. The IMOTHEP project gathers specialists from every field of hybrid-electric propulsion, allowing direct exchanges between aircraft designers and components designers. One of the challenges faced in IMOTHEP was that technology improvement was expected by the component designers, but the direction for improvements was to be given by aircraft designers. Depending on the requirements set by the aircraft designer, the component designer would select one solution and provide performance estimations for state-of-the-art and future available technology. In this situation, one of the goals of preliminary aircraft analysis is to identify minimum technology levels, making the configuration

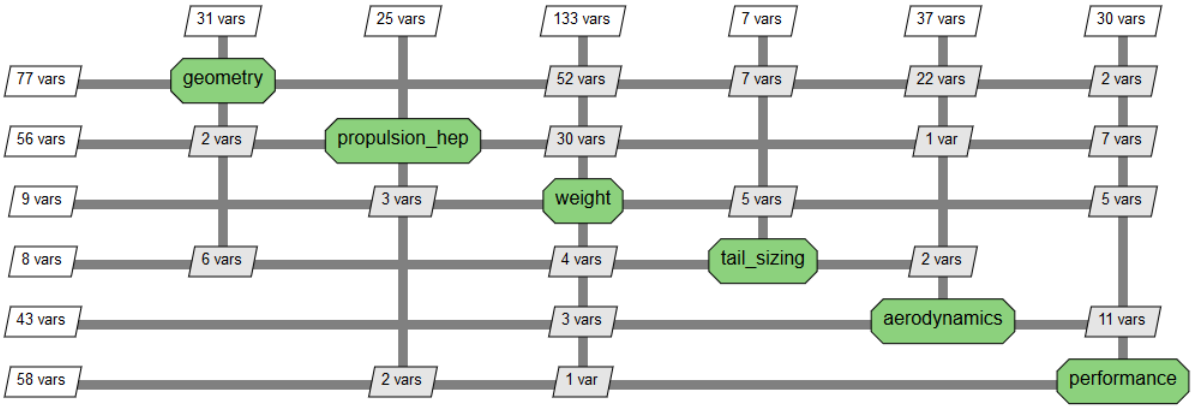

Fig. 2 DRAGON design process.

viable or profitable compared to a reference aircraft. These minima are then communicated to component designers and may be set as targets for future research. The aircraft designer is hence particularly interested in the design sensitivities to set targets and priorities in the development of new technologies.

In the particular case of the DRAGON concept, discussions within the multi-disciplinary design team of the IMOTHEP project led to the following questions:

- For each electrical component, specific power (kW/kg), power density (kW/L) and efficiency are the result of a trade-off. For example, a very dense motor is more difficult to cool down, so heavier cooling equipments are required and the efficiency is negatively impacted. In the development of components dedicated to commercial aviation, which parameter should be prioritized?
- Employing high voltage levels (more than 1kV) is a challenge for an aircraft flying at a high altitude. It is usually viewed as a long-term technology improvement. How does this parameter compare with respect to the other, more easily achievable technology improvements?
- Finally, what is the relative impact of electric components improvements versus an increase in gas turbine efficiency?

B. Turbo-electric component characteristic

The input variables of interest correspond to the characteristics of turbo-electric components, including the Electrical Power Unit (EPU), which consists of the electric motor and power electronics, as well as power generation and power transmission. Specifically, the characteristics consist of the specific power, power density, and efficiency of the EPU and power generation, along with the turboshaft Power Specific Fuel Consumption (PSFC) and the voltage for power transmission. The fan is designed considering a fixed fan pressure ratio of 1.2. It is not part of the input variables as no

activity was planned for detailed fan design of the SMR-CON concept within the IMOTHEP project. Table 1 shows the definition of the input variables and the associated bounds for the propulsive components studied in this paper. The bounds were selected based on component design exercises but also account for future technology developments (see [25] for details about EPU designs and [29] for details about generator designs). From the point of view of aircraft performance, it is of interest to have compact, light and efficient components. Therefore one would aim at: (i) increasing specific power, power density and efficiency, (ii) increasing the voltage level, which reduces the size and number of parallel cables, (iii) decreasing the turboshaft PSFC, expressed in fuel mass flow rate per output power [kg/kWs], it is inversely proportional to the turboshaft thermal efficiency.

Table 1 Variables and associated bounds for the propulsive components used in this study.

Component	Characteristics	Nominal	Min.	Max.
EPU	Specific power (kW/kg)	9.2	4.6	15
(Electric motor + inverter)	Power density (kW/L)	5	3.8	20
	Efficiency	0.967	0.96	0.99
Power generation	Specific power (kW/kg)	6.55	6	10
(Generator + converter)	Power density (kW/L)	11	3.8	15
	Efficiency	0.97	0.96	0.99
Turboshaft	PSFC Multiplier	1	0.885	1.04
Power transmission	Voltage (V)	3000	1000	3000

A Design Of Experiments comprising 200 points sampled by Latin Hypercube Sampling [30] was generated. For each of the 200 points, an aircraft is sized with a multi-disciplinary design framework (refer to Fig. 1). So, each point represents a different aircraft sized with a different set of input variables listed in Table 1. Three quantities of interest are then extracted: the maximum lift-to-drag ratio $(L/D)^*$, the operating empty weight (OEW) and the fuel burn (FB). The primary objective is to minimize the FB, so this quantity will tell in which direction the research should go. The OEW can be regarded as a secondary objective as it reflects the acquisition cost of the aircraft and the L/D ratio will capture the couplings between propulsion and aerodynamics. Both the OEW and the L/D impact the FB and will help understand the motivations behind the research direction. For the purpose of design exploration, surrogate models need to be constructed to capture the relationship between the propulsive component characteristics and the three QOIs. In the following section, we provide an explanation of the surrogate model methodology employed, along with the accompanying explainability technique used to conduct design exploration.

*Note that a climbing cruise at the maximum lift-to-drag ratio is performed during the mission simulation.

III. Explainable Surrogate Model

A. Polynomial Chaos Expansion

The non-intrusive PCE surrogate model is employed to approximate the relationship between the eight input variables and the three outputs corresponding to the performance.

Let us first define $\boldsymbol{x} = \{x_1, x_2, \ldots, x_m\}^T$ as the vector of input variables, where m is the input dimensionality. Specifically, we are interested in cases with $m > 1$. The objective is to approximate $y = f(\boldsymbol{x})$ with a surrogate model $\hat{f}(\boldsymbol{x})$, that is, $\hat{f}(\boldsymbol{x}) \approx f(\boldsymbol{x})$. The input domain is assumed to be on the m-dimensional hyperbox $\boldsymbol{\Omega} = \prod_{i=1}^{m} \Omega_i$, where $\Omega_i = [0, 1]$. It is worth noting that any hyperbox with arbitrary bounds can be normalized to $[0, 1]^m$. The PCE represents $\hat{f}(\boldsymbol{x})$ with a sum of orthogonal polynomials, which are truncated to a certain number of bases:

$$f(\boldsymbol{x}) = \sum_{i=0}^{\infty} \alpha_i \Psi_i(\boldsymbol{x}) \approx \hat{f}(\boldsymbol{x}) = \sum_{i=0}^{P} \alpha_i \Psi_i(\boldsymbol{x}), \tag{1}$$

where Ψ_i is the i-th multi-dimensional orthogonal polynomial basis and $P + 1$ is the size of polynomial bases set. It is necessary first to collect the experimental design $\boldsymbol{\mathcal{X}} = \{\boldsymbol{x}^{(1)}, \boldsymbol{x}^{(2)}, \ldots, \boldsymbol{x}^{(n)}\}^T$, where n is the number of sampling points, and the responses $\boldsymbol{y} = \{f(\boldsymbol{x}^{(1)}), \ldots, f(\boldsymbol{x}^{(n)})\}^T$. Let us also define the set $\mathcal{I}_p$ with cardinality $P + 1$ comprising the index set for the polynomial bases. We can then use the following notations to denote the PCE approximation:

$$f(\boldsymbol{x}) \approx \hat{f}(\boldsymbol{x}) = \sum_{\boldsymbol{\vartheta} \in \mathcal{I}_p} \alpha_{\boldsymbol{\vartheta}} \Psi_{\boldsymbol{\vartheta}}(\boldsymbol{x}), \tag{2}$$

where $\boldsymbol{\vartheta} = \{\vartheta_1, \vartheta_2, \ldots, \vartheta_m\}$, $\vartheta \geq 0$ is an individual index, and $\boldsymbol{\alpha} = \{\alpha_0, ..., \alpha_P\}$ is the corresponding PCE coefficients. Using this notation, a multi-dimensional polynomial basis can be defined as follows:

$$\Psi_{\boldsymbol{\vartheta}} = \prod_{j=1}^{m} \psi_{\vartheta_j}(x_j), \tag{3}$$

where $\psi_{\vartheta_j}(x)$ is a one-dimensional orthogonal polynomial. Assuming that $\boldsymbol{x}$ lives on an m-dimensional unit hypercube with uniform distribution (i.e., $x_i \sim \mathcal{U}(-1, 1)$) and independency between all input variables, the orthogonal polynomials that suit the purpose are multivariate Legendre polynomials, which are orthogonal with respect to the uniform distribution. For non-uniform standard distributions, other orthogonal polynomials derived from the Askey Scheme should be used [31]. To generate the index set $\mathcal{I}_p$, where $p \geq 0$ is the polynomial order (in practice, $p > 0$ is always used), the hyperbolic truncation is utilized, defined as follows:

$$\mathcal{I}_p \equiv \{\boldsymbol{\vartheta} \in \mathbb{N}^m : \|\boldsymbol{\vartheta}\|_q \leq p\}, \tag{4}$$

where q is the coefficient that allows further truncation of the polynomial basis set, reads as

$$\|\boldsymbol{\vartheta}\|_q = \left(\sum_{i=1}^{m} \vartheta_i^q \right)^{1/q}, 0 < q \leq 1. \tag{5}$$

Using $\mathcal{I}_p$ and the pair of experimental design $\mathcal{D} = \{\boldsymbol{\mathcal{X}}, \boldsymbol{y}\}$, the $n \times P$ information matrix $\mathbf{F}$, where $F_{ij} = \Psi_j(\boldsymbol{x}^{(i)}), i = 1, 2, \ldots n$ and $j = 1, 2, \ldots, P$, can be constructed. Solving $\mathbf{F}\boldsymbol{\alpha} = \boldsymbol{y}$ would yield the PCE coefficients. The standard least square solver requires $n > P$ to ensure stable computation. In this paper, we employ the least angle regression (LARS) algorithm [10, 32] from the UQLab package [33] to find the sparse representation of the function so that it is possible to set $P > n$.

The model's accuracy was assessed using the leave-one-out cross-validation (LOOCV) error, reads as

$$\varepsilon_{LOO} = \frac{\sum_{i=1}^{n} \left(f(\boldsymbol{x}^{(i)}) - \hat{f}_{-i}(\boldsymbol{x}^{(i)}) \right)^2}{\sum_{i=1}^{n} (f(\boldsymbol{x}^{(i)}) - \hat{\mu}_f)^2} \tag{6}$$

where $\hat{f}_{-i}(\boldsymbol{x}^{(i)})$ refers to the PCE model constructed using all data points in $\mathcal{D}$ excluding the i-th data point (i.e., $\boldsymbol{x}^{(i)}$), and $\hat{\mu}_f = \frac{1}{n} \sum_{i=1}^{n} f(\boldsymbol{x}^{(i)})$ denotes the sample mean of the responses at $\mathcal{D}$. The denominator in Eq. (6) corresponds to the squared differences between the actual response and the mean response across all samples. Consequently, ε_{LOO} serves as the normalized version of the LOOCV error, ensuring that it remains unaffected by the scale of the response variable.

B. Shapley Additive Explanations for a PCE model

In this paper, we refer to the explanations of SHAP outlined in Palar *et al* [16], which is specific to a PCE model. First, we establish the following notations: Let $[1:m]:1,2,\ldots,m$, and we define a subset as u such that $u \subseteq [1,2,\ldots,m]$. The complement of u is denoted as $-u$ and is defined as the set $[1:m]$ with all elements of u removed. The size of the subset u is represented as $|u|$. We can then define $\boldsymbol{\Omega}_u$ to indicate the subset of $\boldsymbol{\Omega}$ that corresponds to the index set u; that is, $\boldsymbol{\Omega}_u = \prod_{i \in u} \Omega_i$. Using the above notation, we can represent the PCE model as follows:

$$\hat{f}(\boldsymbol{x}) = \sum_{u \subseteq [1:m]} \hat{f}_u(\boldsymbol{x}_u), \tag{7}$$

where $\hat{f}_\emptyset = \mathbb{E}[\hat{f}(\boldsymbol{x})]$, where $\mathbb{E}(.)$ is the expectation operator, and, obviously, $\hat{f}_{[1:m]} = \hat{f}(\boldsymbol{x})$. The SHAP decomposition works as follows:

$$\hat{f}(\boldsymbol{x}) = \hat{f}_\emptyset + \sum_{j=1}^{m} \phi_j(\boldsymbol{x}), \tag{8}$$

where ϕ_j is the input attribution (i.e., SHAP values) for the j-th input variable. Let us define $\underline{\hat{f}}_u(\boldsymbol{x}_u)$ which comprises all subset variables in u:

$$\underline{\hat{f}}_u(\boldsymbol{x}_u) = \sum_{v \subseteq u} \hat{f}_v(\boldsymbol{x}_v), \tag{9}$$

For $j = 1, 2, \ldots m$, the SHAP input variable at a specific input point $\boldsymbol{x}^*$ can be computed as follows:

$$\phi_j(\boldsymbol{x}^*) = \frac{1}{m} \sum_{u \subseteq \{-j\}} \binom{m-1}{|u|}^{-1} \left(\underline{\hat{f}}_{u \cup \{j\}}(\boldsymbol{x}^*) - \underline{\hat{f}}_u(\boldsymbol{x}^*) \right), \tag{10}$$

where $\{-j\} = [1 : m] \setminus j$, representing the set containing all input variables excluding the j-th input variable. The Shapley value for the j-th input variable represents the average marginal contribution of the j-th input to the difference in predictions of the surrogate model when adding it to different subsets of input variables. In essence, Eq.(10) quantifies the importance of the j-th input variable in the surrogate model's prediction considering all possible combinations. Using the SHAP decomposition shown in Eq. (8), it has been shown that the SHAP values from a PCE model can be computed analytically without any approximation technique. The expression reads as

$$\phi_j(\boldsymbol{x}^*) = \frac{1}{m} \sum_{u \subseteq \{-j\}} \binom{m-1}{|u|}^{-1} \left(\sum_{\boldsymbol{\vartheta} \in \mathcal{K}_{u,j}} \boldsymbol{\alpha}_{\boldsymbol{\vartheta}} \boldsymbol{\Psi}_{\boldsymbol{\vartheta}}(\boldsymbol{x}^*) \right), \tag{11}$$

where $\mathcal{K}_{u,j}$ is the set of $\boldsymbol{\vartheta}$ tuples such that

$$\mathcal{K}_{u,j} = \left\{ \|\boldsymbol{\vartheta}\|_0 \leq |u \cup \{j\}|, \boldsymbol{\vartheta} : \begin{array}{ll} \vartheta_j > 0 & \\ \vartheta_k = 0 & \forall k = 1, \ldots, m \quad k \notin (u \cup \{j\}) \end{array} \right\}. \tag{12}$$

Finally, the averaged SHAP values can be computed as follows:

$$\bar{\phi}_j = \mathbb{E}(|\phi_j(\boldsymbol{x})|) \approx \frac{1}{n_m} \sum_{i=1}^{n_m} |\phi_j(\boldsymbol{x}^{(i)})|, \tag{13}$$

where the averaging is performed across n_m samples generated in the input space $\boldsymbol{\Omega}$. The averaged SHAP values act as a GSA metric that quantifies the average contribution of input variables on the prediction of a surrogate model. In some plots, we also show the normalized average SHAP values, which are obtained by dividing the averaged SHAP value by the maximum $\bar{\phi}$ for the corresponding quantity of interest.

The SHAP values obtained from a PCE model serve multiple purposes. Firstly, they are mainly used to assess the influence of each input variable concerning the trend. This information proves valuable in exploring potential interactions between variables and nonlinearity, which can be visually represented using the SHAP dependence plot. It is essential to note that Sobol indices cannot reveal such insights, as they do not offer information about the specific

shape or behaviour of the underlying function. Secondly, the averaged SHAP values offer insights into the significance of each input on the output, similar to Sobol indices.

In conjunction with SHAP, we also computed the Sobol indices to be compared with the averaged SHAP values. Additionally, the Sobol indices are used to assess potential interactions between input variables concerning their impact on the QOIs. The first and total Sobol indices are denoted as S_F and S_T, respectively. In this paper, we refrain from going into the intricate details of Sobol indices to maintain conciseness and avoid making the paper overly lengthy. More details on Sobol indices can be found in dedicated literature [21].

C. Correlation coefficients

Another useful information we can derive from SHAP is the correlation between various quantities. Such information is useful to help understand the relationship between two variables of interest in terms, that is, whether they move together (positive correlation), in opposite directions (negative correlation), or not correlated at all. Analyzing the correlation between sample values and their corresponding SHAP values for a specific QOI provides insights into how changes in input variables influence the QOI's direction. On the other hand, the correlation between SHAP values of two distinct QOIs, both functions of a particular input variable, reveals whether changes in that input variable cause the two QOIs to move together or in opposite directions.

Let us denote arbitrary variables ξ and ζ, which can represent the sample values or SHAP values; the Pearson correlation coefficient between the two variables (i.e., $\rho_{\xi,\zeta}$) is calculated as:

$$\rho_{\xi,\zeta} = \frac{\sum_{i=1}^{n_s} \left[(\xi^{(i)} - \bar{\xi})(\zeta^{(i)} - \bar{\zeta})\right]}{\sqrt{\sum_{i=1}^{n_s} (\xi^{(i)} - \bar{\xi})^2 \sum_{i=1}^{n_s} (\zeta^{(i)} - \bar{\zeta})^2}}, \tag{14}$$

where n_s is the sample size, $\bar{\xi}$ is the mean of the ξ-variable, and $\bar{\zeta}$ is the mean of the ζ-variable . The Pearson correlation coefficient measures the linear dependency between ξ and ζ. Thus, it can be used to check whether the change in ξ affects ζ linearly. Perfect Pearson coefficient (i.e., $|\rho_{\xi,\zeta}| = 1$) indicates that the relationship is perfectly linear. If $|\rho_{\xi,\zeta}| < 1$, the relationship departs from linearity.

The Spearman correlation coefficient ($s_{\xi,\zeta}$), on the other hand, checks the monotonous relationship between two variables. To calculate this coefficient ($s_{\xi,\zeta}$), the variables ξ and ζ are first converted to ranks $R(\xi^{(i)})$ and $R(\zeta^{(i)})$ for each sample, respectively. The Spearman correlation coefficient is then computed as

$$s_{\xi,\zeta} = 1 - \frac{6 \sum_{i=1}^{n_s} d_i^2}{n_s(n_s^2 - 1)}, \tag{15}$$

where $d_i = R(\xi^{(i)}) - R(\zeta^{(i)})$ represents the difference between the ranks of each sample. Perfect Spearman correlation (i.e., $|s_{\xi,\zeta}| = 1$) indicates a monotonic relationship, whether it is a linear dependency or not. Conversely, $|s_{\xi,\zeta}| < 1$

shows departure from monotonicity.

IV. Results and Discussions

In this section, we detail the analysis of the constructed surrogate models, GSA, and detailed SHAP analysis. For ease of reading in the figure results, Table 2 displays the shortened names of the variables.

Table 2 Notations for the eight input variables for the propulsive components used in this study.

Component	Characteristics	Notation
EPU	Specific power (kW/kg)	EPU spe. pow.
(Electric motor + inverter)	Power density (kW/L)	EPU pow. dens.
	Efficiency	EPU eff.
Power generation	Specific power (kW/kg)	POW spe. pow.
(Generator + converter)	Power density (kW/L)	POW pow. dens.
	Efficiency	POW eff.
Turboshaft	Multiplier	Turbo SFC
Power transmission	Voltage (V)	Voltage

A. Surrogate model building

We sought the best polynomial bases by applying LARS to the index set from $\mathcal{I}_{p=1}$ to $\mathcal{I}_{p=8}$. Setting a high maximum polynomial order intentionally considers the possibility of strong nonlinearity. The results from the PCE models, including the leave-one-out cross-validation error, maximum polynomial order retained, polynomial order for each input, the sum of first-order indices, and the number of non-zero (NNZ) coefficients, are shown in Table 3.

The results show that the PCE models yielded low normalized LOOCV errors, see Eq. (6), for all three outputs (in the order of 10^{-3}). The high level of accuracy indicates that the PCE models are well-suited for knowledge extraction using SHAP analysis. Furthermore, the results show that the LARS algorithm retains the maximum polynomial order of 4 with non-zero coefficients for some variables, indicating nonlinearity in the input-output relationship. However, it is worth noting the coefficients of the retained higher polynomial orders (i.e., higher than the second order) are relatively small compared to the lower orders, as shown in Fig. 3. It can also be seen that the input-output relationships are "compressed", where the magnitude of low-order polynomials tends to surpass that of higher-order polynomials. While the coefficients provide some information, comprehending the mechanisms governing the relationships between each input and output remains challenging; such intricacy is further revealed through SHAP analysis. Furthermore, the sum of the first-order Sobol indices in Table 3, which is close to one, suggests that the interactions between variables are weak. This essentially means that the three QOIs are close to purely additive functions. In other words, the impact of each propulsive component characteristic is almost independent of each other regarding its effect on all QOIs. This makes sense from the point of view of turbo-electric propulsion, considering the simple modelling used for electric

components. Each input has a direct and main effect on one of the QOIs. The specific power directly impacts OEW, the power density mainly the wetted area and through it the L/D ratio, the efficiencies directly impact the fuel burn. With the current physical models, varying the specific power or the power density of electric components has no effect on their efficiencies. More discussions on the GSA results are shown in the next section.

Table 3 Description of the constructed PCE models for the three QOIs.

Output	ε_{LOO}	p_{max}	Poly. order	$\sum S_{F_i}$	NNZ
L/D	4×10^{-3}	4	[3, 4, 2, 2, 2, 3, 2, 4]	0.996	43
OEW	5.7×10^{-3}	4	[3, 3, 2, 2, 2, 2, 2, 4]	0.993	43
Fuel burn	2.5×10^{-3}	4	[3, 3, 2, 2, 2, 1, 2, 3]	0.995	48

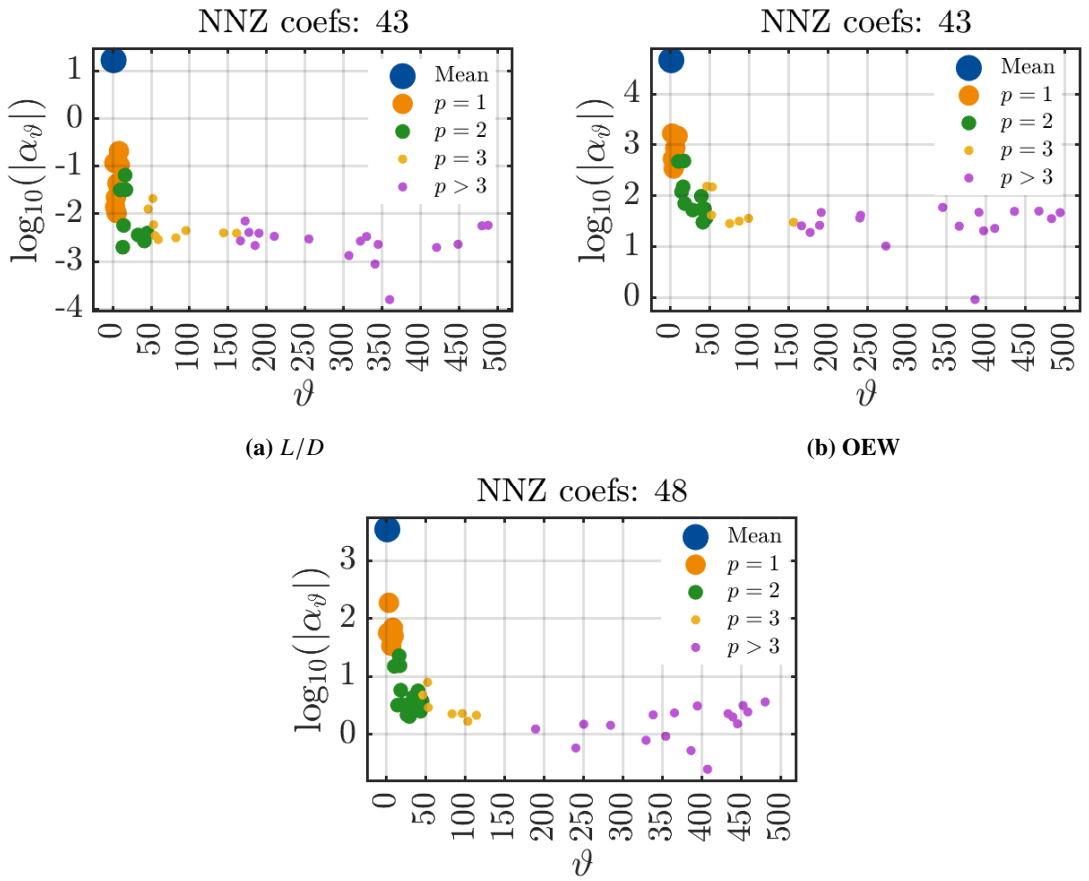

(a) L/D **(b) OEW**

(c) Fuel burn

Fig. 3 Magnitude of the PCE coefficients for the three outputs (NNZ stands for number of non-zero coefficients).

B. Global sensitivity analysis

Before delving further into the dependency of the QOIs on the input variables, we conducted an analysis of the GSA metrics to determine the significance of each input variable. Two GSA metrics are used, namely, Sobol indices and

averaged SHAP values. The Sobol indices and the averaged SHAP values computed from the PCE models are shown in Figs. 4 and 5, respectively. First, it can be seen that the relative magnitude of Sobol indices appears larger than averaged SHAP values. The reason is that Sobol indices are squared quantities, which is not the case for averaged SHAP values. In the context of this problem, we think that the averaged SHAP values make more sense since the input variables are deterministic and not random, although uniform distributions are assumed for all inputs since it is necessary for PCE construction. Moreover, while Sobol indices might seem intuitive at first glance, they lack clarity in terms of quantifying the actual change produced when the input variables are altered (given the allowable range of the inputs). The averaged SHAP values offer greater intuitiveness in the context of design exploration as they provide a clearer understanding of how individual input variables, on average, contribute to and impact the model's output. Besides, the averaged SHAP values maintain the same unit as the original quantity of interest. In general, for all QOIs, both GSA metrics agree on

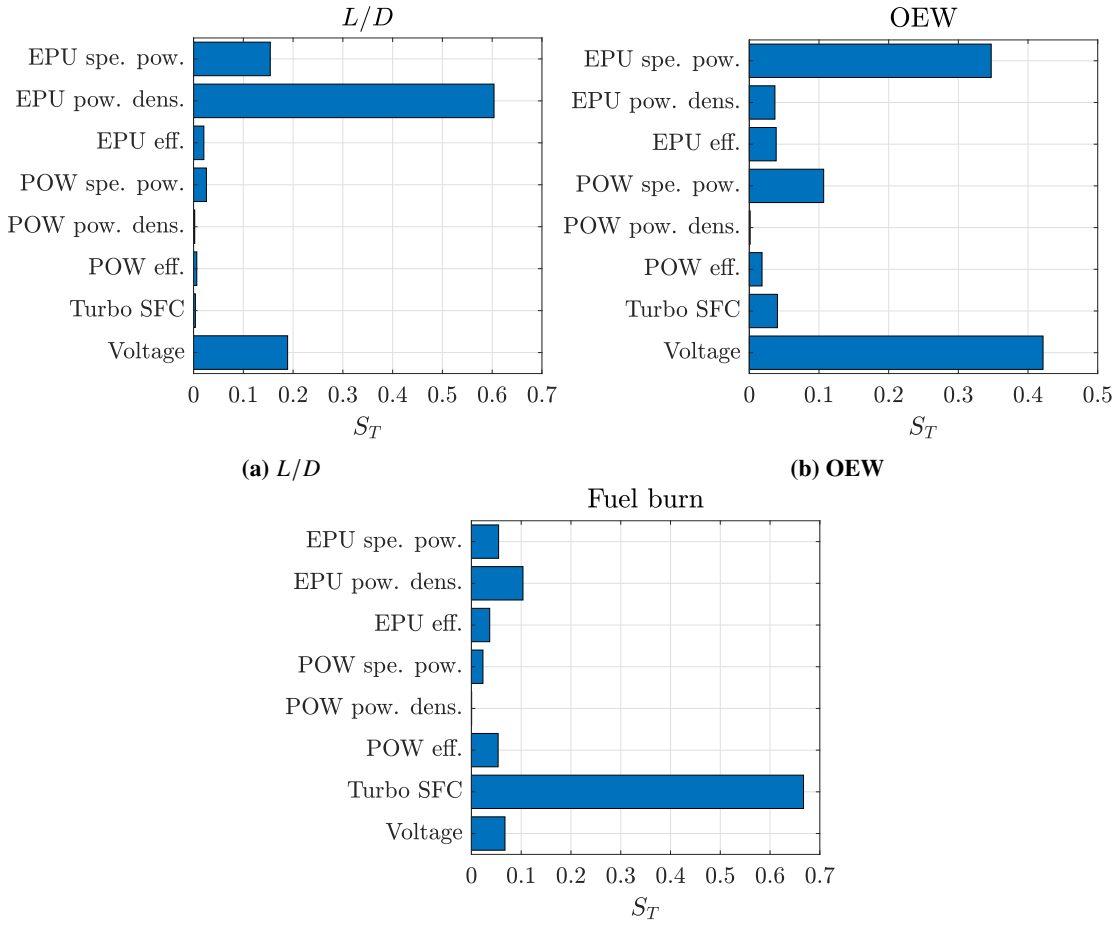

(a) L/D **(b) OEW**

(c) Fuel burn

Fig. 4 Total Sobol indices extracted from PCE for the three QOIs.

the ranking of input variables in terms of their importance. There is only one slight disagreement on how averaged SHAP and Sobol index perceive the importance of EPU-specific power and POW-efficiency on fuel burn. However, the

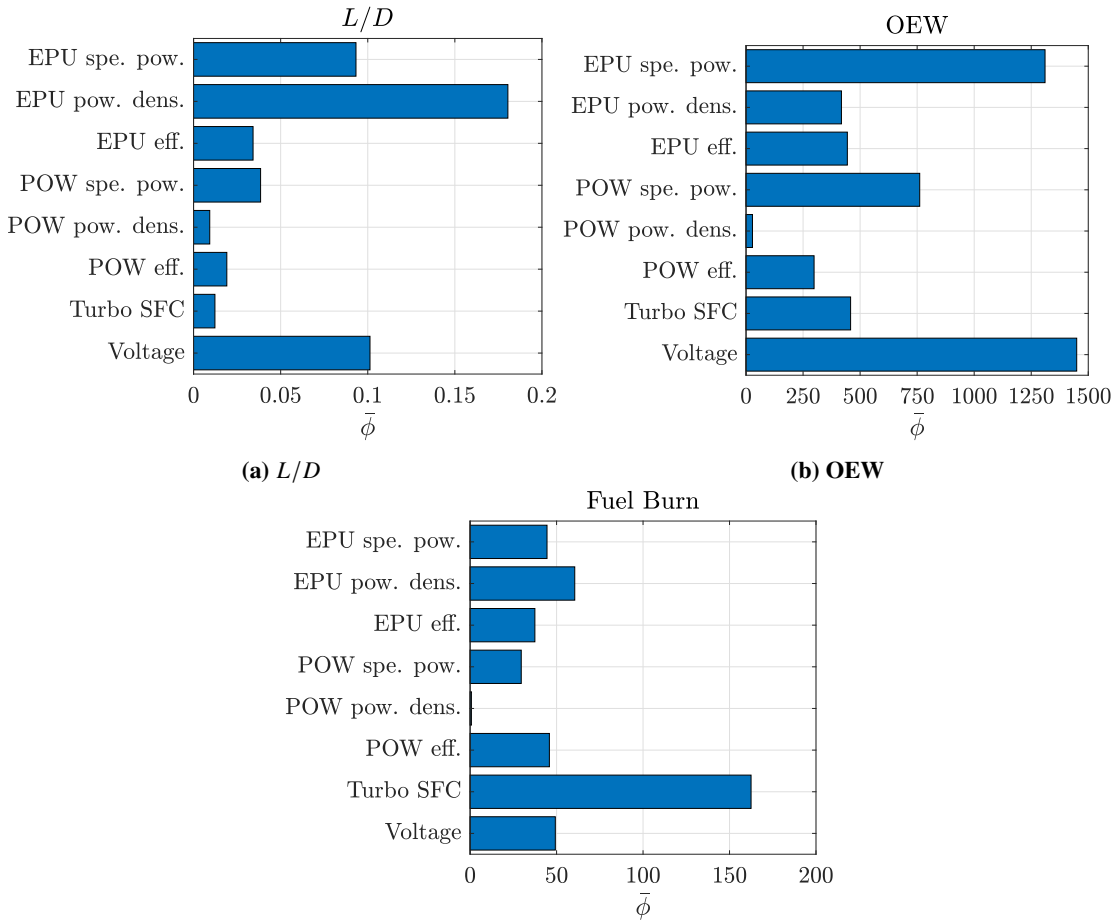

(a) L/D **(b) OEW**

(c) Fuel burn

Fig. 5 Averaged SHAP values extracted from PCE for the three QOIs.

difference is slight, and it is acceptable to say that both variables are equal in terms of importance. The EPU-power density is the most important variable affecting L/D, followed by EPU-specific power and voltage, which are roughly equal in importance. The Sobol indices perceive that the EPU-specific power and voltage are approximately four times less important than EPU-power density. However, the importance magnitude of both variables is perceived to be half that of EPU-power density according to the averaged SHAP values. The rest of the variables are much less influential than others in how they affect L/D. Regarding OEW, the two most critical variables are EPU-specific power and voltage, with POW-specific power ranking closely behind. The influence of EPU-power density, EPU efficiency, and turbo SFC on OEW can be deemed comparable. The impact of POW-efficiency is small but not negligible, especially from the viewpoint of its averaged SHAP value. Finally, POW-power density does not significantly impact OEW; in fact, its impact is not significant for any of the QOIs. This may come as a surprise compared to the high impact of EPU power density. It is explained by the fact that the nacelle of the turbo-generator has a much larger diameter than the hub of the electric fans (where the EPU are located). Consequently, the ratio of wet area over volume is much more favourable to

the turbo-generator, to the point that the power density has a very small impact on drag. Among the variables examined, Turbo SFC stands out as the most influential factor affecting fuel burn, displaying a notably stronger effect than the others. While the impact of the remaining variables on fuel burn is relatively similar, the EPU power and voltage are considered more influential than the rest. The only exception is the effect of POW-power density on fuel burn, which is deemed non-significant. Once more, there is a distinct contrast in how both GSA metrics perceive the relative influence of Turbo SFC on fuel burn. However, it is worth noting again that the current problem is not random (hence, there is no randomness associated with the input variable). Consequently, utilizing averaged SHAP to evaluate the importance of inputs in the current problem is more sensible than relying on Sobol indices.

The GSA metrics provide useful information on the global importance of input variables; however, they do not reveal the individual dependency of how each input affects the QOIs; this is the subject of the discussion in the next section.

C. SHAP summary plot analysis

Figure 6 displays the distribution of the 200 sampling points in the projected two-dimensional output space (i.e., L/D vs fuel burn, L/D vs OEW, and OEW vs fuel burn), along with the corresponding linear correlation coefficient. The figure illustrates the challenge of extracting trends and insights directly from visualizing the output space. A slight positive correlation can be observed between L/D and OEW, while the correlation between L/D and fuel burn appears to be close to zero. Furthermore, although there exists a general trend of reducing OEW leads to reduced fuel burn (as evidenced by the moderate positive correlation of $\rho = 0.64$), analyzing how each input affects the QOIs remains difficult. The drawback of this plotting technique is that it may potentially create a misleading impression, such as suggesting that there is no correlation between L/D and fuel burn. As demonstrated in the following explanations, decomposing each relationship through SHAP decomposition offers a meaningful way to deduce these relationships.

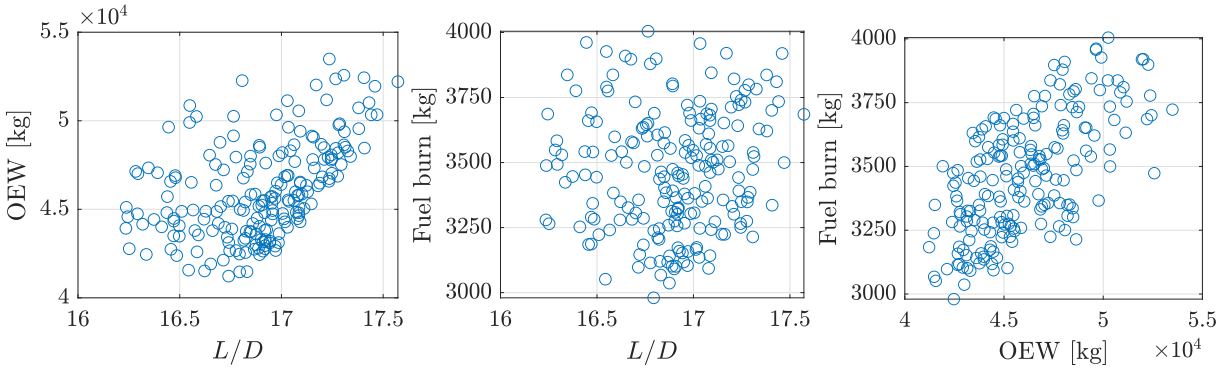

(a) L/D **vs OEW** ($\rho = 0.48$) **(b)** L/D **vs fuel burn** ($\rho = 0.08$) **(c) OEW vs fuel burn** ($\rho = 0.64$)

Fig. 6 Two-dimensional scatter plots of the 200 sampling in the output space

The SHAP summary plots for the three QOIs are shown in Fig. 7. The direction of how each input affects L/D, OEW, and FB is more pronounced in this plot. One important insight obtained is that each input variable strongly

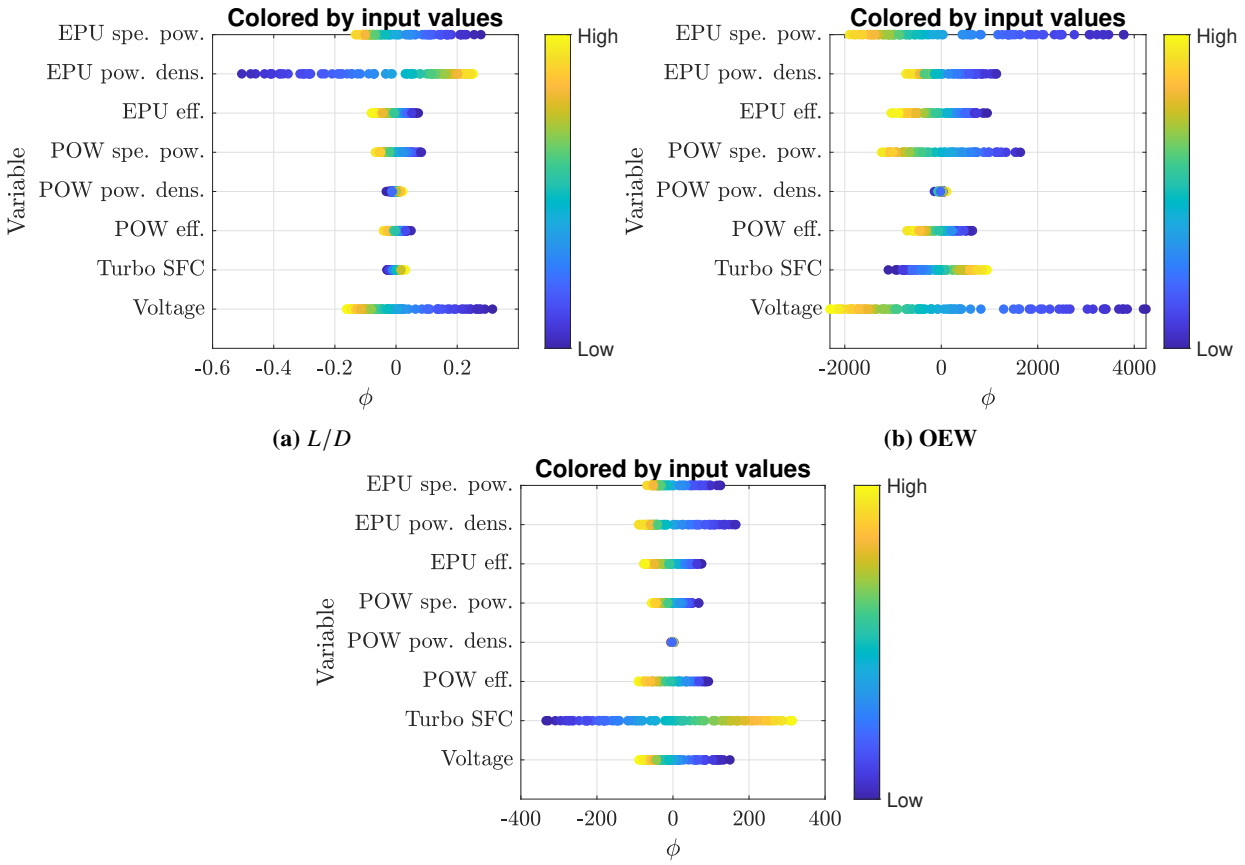

(a) L/D **(b) OEW**

(c) Fuel burn

Fig. 7 SHAP summary plots for the three QOIs.

correlated with the QOIs. Moreover, the arrangement of the colour gradation further suggests that the interaction is weak; a disorganized gradation, on the other hand, indicates strong interaction, non-monotonous relationship, or nonlinearity. Nevertheless, as demonstrated in the subsequent individual SHAP dependence plot, it becomes evident that the impact is nonlinear for certain variables, yet the dependency remains monotonic. The SHAP summary plot facilitates understanding the correlation between the impact of individual variables on multiple QOIs. Specifically, Table 4 presents the linear correlation coefficient between the SHAP values of two QOIs concerning a specific input variable. It is essential to note that this correlation coefficient pertains to the SHAP values of two QOIs, not the correlation between the input variable and the SHAP value for a single quantity of interest, which will be discussed in the next section. When discussing this correlation, it is important to reiterate the magnitude of the input variables again. This is because the correlation measures the dependency without referring to the input importance.

To appreciate the correlations shown in Table 4, Fig. 8 shows the SHAP values of two representative variables, namely EPU specific power and EPU power density, concerning two QOIs (L/D and OEW). The SHAP values of EPU specific power for L/D and OEW exhibit a positive linear correlation (as indicated by the corresponding positive Spearman and Pearson correlation coefficient); in other words, the two QOIs move in the same direction when the

EPU specific power changes. The plot is also more specific, showing that the reduction in EPU specific power would simultaneously increase the L/D and OEW (noting that the other variables are kept fixed). Conversely, as the function of solely EPU power density, the L/D and OEW move in the opposite direction: increasing EPU power density would reduce OEW, but the L/D is increased, and vice versa. The complete plots for all variables are not shown in this paper; however, it should be sufficient to understand the correlation since the absolute values are generally large (i.e., either strong positive or negative correlation). This example also explains the misleading impression that L/D does not correlate with FB. When the OEW and L/D simultaneously increase, the added weight cancels any benefit brought by better L/D. This behaviour takes its origin in the way the aircraft is sized: the wing surface area is calculated using the aircraft weight to satisfy a prescribed approach speed. In turn, a large wing leads to slightly improved aerodynamics. Overall, as the weight increase is more important, the FB seems penalized when L/D improves, but the real cause is the weight increase. The correlations between how the input variables affect L/D and OEW (see $\rho(\phi_{L/D}, \phi_{\text{OEW}})$) and also fuel burn (see $\rho(\phi_{L/D}, \phi_{\text{Fuel Burn})}$) are generally positive, except for the EPU power density (with negative correlation) and power generation power density (with near-zero correlation). The limited correlation attributed to the power density of the power generation arises from its negligible influence on all QOIs. As a result, the SHAP values appear scattered due to their lack of significant impact. The results indicate that an increase in L/D due to the individual impact of all variables except EPU power density (with negative correlation) and power generation power density (with near-zero correlation) leads to a simultaneous increase in OEW and fuel burn, and vice versa.

There is a clear trade-off between how increasing L/D also tends to increase the OEW. In other words, achieving enhanced aerodynamic efficiency comes at the cost of increased system weight. This statement is valid with the considered input variables only and shows again the underlying sizing rule of the wing. Since it is obvious that reducing OEW leads to reduced fuel burn, the direction of how all input variables, except for the power density of the power generation, change OEW positively correlates with the fuel burn (see $\rho(\phi_{\text{OEW}}, \phi_{\text{fuel burn}})$ in Table 4).

Table 4 Linear correlation coefficient between SHAP values of different QOIs as a function of individual input variable

Variable	$\rho(\phi_{L/D}, \phi_{\text{OEW}})$	$\rho(\phi_{L/D}, \phi_{\text{Fuel burn)}})$	$\rho(\phi_{\text{OEW}}, \phi_{\text{fuel burn}})$
EPU spe. pow.	0.9972	0.9953	0.9969
EPU pow. dens.	-0.9939	-0.9978	0.9939
EPU eff.	0.9930	0.9951	0.9950
POW spe. pow.	0.9967	0.9929	0.9945
POW pow. dens.	0.0480	0.0896	0.0041
POW eff.	0.9881	0.9906	0.9910
Turbo SFC	0.9597	0.9639	0.9967
Voltage	0.9987	0.9962	0.9981

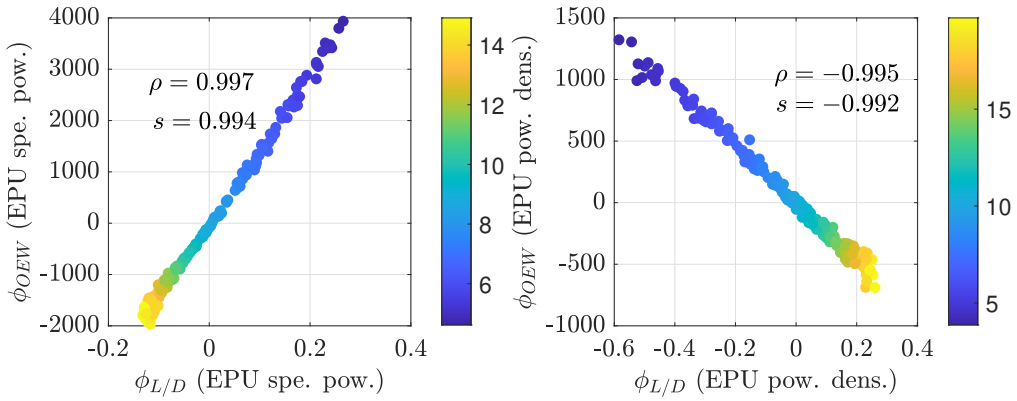

(a) EPU specific power **(b) EPU power density**

Fig. 8 Scatter plots of SHAP values for L/D and OEW as a function of specific variables

D. SHAP dependence plot analysis

The individual SHAP dependence plots illustrate the individual tendencies of the input variables and their impact on the QOIs. To be precise, the individual plot provides additional insights into the level of nonlinearity and, if present, the interaction mechanisms. The analysis should be performed while referring to the input importance.

Figure 9 shows all single-variable SHAP dependence plots in a single figure, where the input variables are normalized into $[0, 1]$. The normalized and combined plots better show the relative tendency of all input variables simultaneously. Additionally, the zero SHAP value refers to the zero deviation from the mean of the function. The individual SHAP dependence plots are shown in Appendix B, providing a detailed visual representation of how each input variable influences the model's predictions. First, we observe that the eight input variables affect all QOIs monotonously, i.e., strictly increase or decrease. The results show that some variables exhibit nonlinear tendencies. For all QOIs, it can be seen that the EPU-power density affects L/D in a nonlinear fashion, where it can be seen that the gradient of the corresponding SHAP values changes as the input is changed. The voltage and EPU-specific power also change all QOIs nonlinearly, in which the gradient becomes steeper when the respective values are small. Conversely, as voltage and EPU-specific power reach moderate to high values, their effects tend to approximate linearity. Some variables have traces of small interaction, such as POW-power density and turbo PSFC (see Appendix B for more detailed plots).

E. Consequences for turbo-electric propulsion

The SHAP analysis is particularly useful to set design objectives for each of the component considered in this study. In this section, we will focus on the information provided by SHAP that cannot be obtained with the Sobol analysis.

It has already been seen in Fig. 4 and Fig. 5 that the averaged SHAP values give the same information as the Sobol indices, that is the relative importance of the inputs on the variability of the output. This information can be used to give design priorities; for example, one should put EPU power density improvement as a top priority before EPU-specific power and efficiency improvement. However, this information is only general and does not tell how much improvement

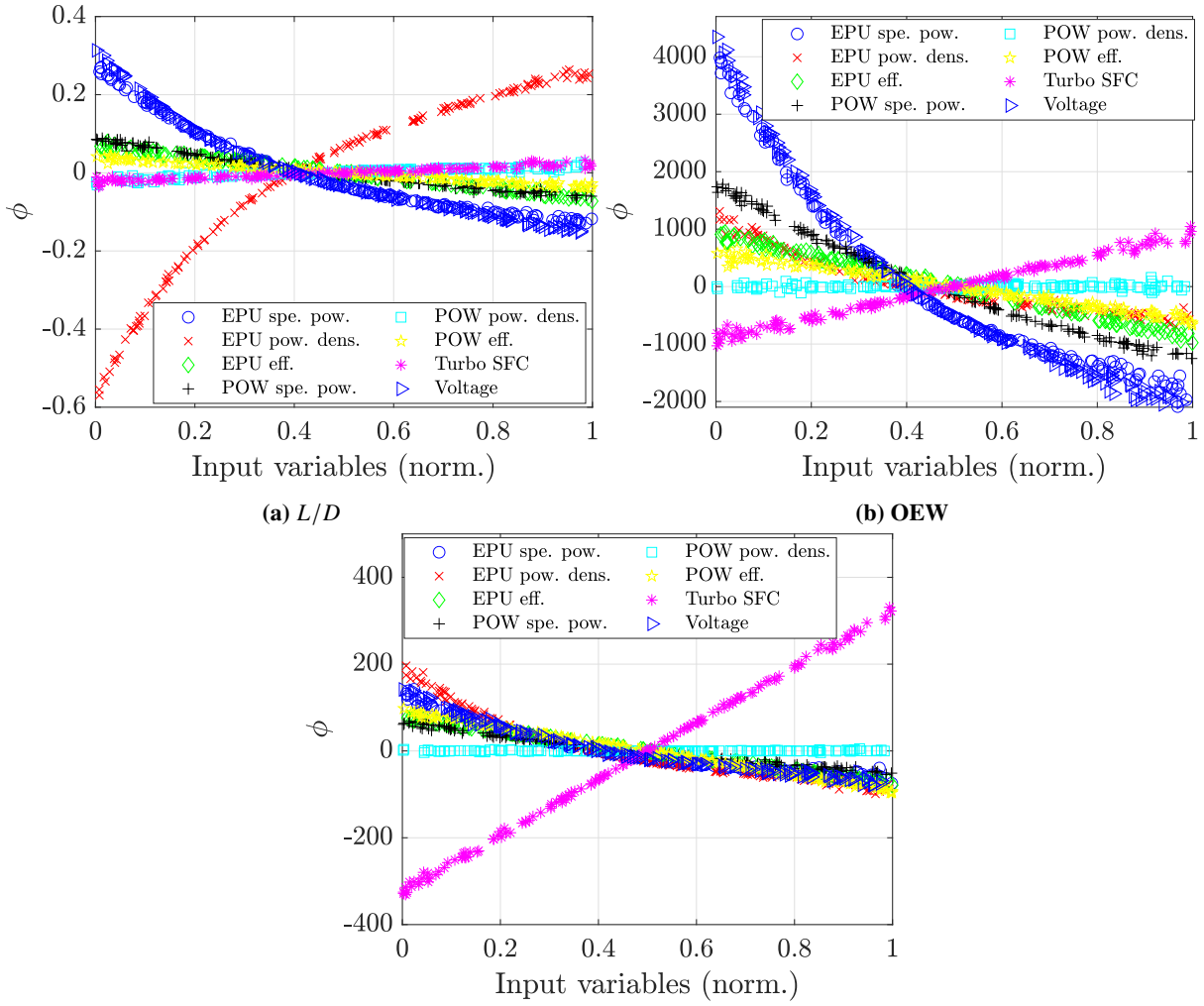

(a) L/D **(b) OEW**

(c) Fuel burn

Fig. 9 Combined SHAP dependence plots for all QOIs with normalized input values.

is desirable. Figure 9 provides the information allowing to set precise design goals and the expected improvement in the aircraft performance. The non-linearity observed in the figures shows where the improvements most impact aircraft performance. Specifically, one can deduce a tipping point from the figures, where the gradient becomes minimum:

- Improving the EPU power density from a minimum 3.8 kW/L up to 10 kW/L allows a fuel burn reduction of 200 kg. Pursuing the improvement effort up to 20 kW/L only brings an additional fuel saving of 100 kg.
- Improving the EPU specific power from the minimum 4.6 kW/kg up to 10 kW/kg allows a fuel saving of 150 kg while going from 10 kW/kg to 15 kW/kg allows only 25-50 kg additional fuel savings.
- Increasing the voltage up to 2 kV allows 150 kg of fuel savings while increasing up to 3 kV brings an additional fuel saving of ~ 50 kg.

When a linear behaviour is observed over the whole range of variation, then sensitivity can be expressed very simply:

- A 1% efficiency gain on EPU translates in ~ 50 kg fuel saving.
- A 1% efficiency gain in Power generation translates in ~ 70 kg of fuel saving.
- A 1% turboshaft PSFC increase translates in ~ 40 kg fuel burn increase.
- Finally, an increase of power generation specific power of 1 kW/kg translates as a ~ 40 kg fuel saving.

We can observe a difference in how the component efficiencies affect the overall performance of the aircraft; this may sound strange as the final performance of the propulsion is obtained by the multiplication of all efficiencies. However, the reader should keep in mind that the aircraft is always resized for each set of inputs. Therefore, the so-called “snowball" effect is taken into account through these different sensitivities. Such quantitative information cannot be obtained with GSA and allows to write precise requirements for component design such as, for the EPU:

- Specific power $\geq$ 10 kW/kg,
- Power density $\geq$ 15 kW/L,
- Efficiency: best achievable while ensuring the two previous requirements.

Because the interaction between input variables is very small, the expected impact of the previous requirements can be estimated by the addition of the effect of a single variable. Therefore, the expected fuel burn reduction of combined EPU-specific power and power density improvement (starting from their lower bound) is around 400 kg, and each percent increase in EPU efficiency will add approximately 50 kg. In previous studies, some of the information could be deduced only qualitatively from 2D plots if the sensitivity was large enough (for example, the EPU power density). However, dominant input variables, such as the turboshaft SFC here, could hide the effect of other less sensitive variables.

V. Conclusions and future works

This study aims to perform a design exploration of the impact of propulsive component parameters on the performance of distributed propulsion. Specifically, our research investigates intricate relationships between the input variables associated with turbo-electric component characteristics and three essential quantities of interest: lift-to-drag ratio, operating empty weight, and fuel burn. The input turbo-electric components included in the analysis encompass specific power, power density, and efficiency of the EPU and power generation, as well as the Turboshaft PSFC and the voltage utilized for power transmission.

The design exploration is made possible through the framework of an explainable PCE surrogate model, which gives essential information on the input-output relationship of a distributed propulsion system. In particular, the SHAP values offer insights into the global input importance, nonlinearity, and correlations between multiple quantities in a manner that conventional exploration methods cannot achieve. First, the averaged SHAP values provide guidance

on the prioritization of input variables concerning the three quantities of interest. The study finds that EPU power density significantly influences L/D, with EPU-specific power and voltage also playing important roles. However, in terms of OEW, EPU-specific power and voltage emerge as critical factors, while turboshaft PSFC notably affects fuel burn. The powerful aspect of SHAP lies in how it quantifies and visualizes the individual impact of each turbo-electric component's characteristics on the three QOIs. Most notably, SHAP identifies the nonlinearity in the quantities of interest, attributed to the impact of EPU-specific power, EPU power density, and voltage. Further, we observe that the impact of each turbo-electric component characteristic on the three quantities of interest remains largely independent, enabling an easy understanding of their respective contributions to the overall performance of the DEP system.

Future research endeavours should focus on several areas. Firstly, there is a need to optimize turbo-electric component characteristics to enhance DEP system efficiency further. The current design exploration can also be readily deployed to investigate advanced propulsion systems, such as hydrogen-powered aircraft. Finally, evaluating the environmental impact is also important and should be included in the design exploration pipeline.

Acknowledgements

This work is part of the activities of ONERA - ISAE - ENAC joint research group. Pramudita Satria Palar acknowledges the financial support provided by Institut Teknologi Bandung under the Riset ITB 2023 program for this research. The authors thank the IMOTHEP project, financed by the European Union's Horizon 2020 Research and Innovation program under Grant agreement No 875006, for the availability of the data.

A. Pedagogical example on the six-variable OTL circuit function

To illustrate how the combination of SHAP and PCE can be useful for knowledge extraction, we applied the framework to the six-variable output transformerless (OTL) push-pull circuit function [34]. The function is written as:

$$V_m(\mathbf{x}) = \frac{(V_{b1} + 0.74)\,\beta\,(R_{c2} + 9)}{\beta\,(R_{c2} + 9) + R_f} + \frac{11.35 R_f}{\beta\,(R_{c2} + 9) + R_f} + \frac{0.74 R_f \beta\,(R_{c2} + 9)}{\left(\beta\,(R_{c2} + 9) + R_f\right) R_{c1}}, \tag{16}$$

where $V_{b1} = (12R_{b2})/(R_{b1} + R_{b2})$. Table 5 shows the definition of the input variables and the corresponding range for the demonstration, with the output of interest being the midpoint voltage V_m. As seen from Eq. (16), it is hard to decipher the individual impact of each input variable on the output.

In this pedagogical example, we show the six SHAP dependence plots (one for each variable) in a single plot (see Fig. 10). However, it is possible to present the SHAP dependence plot individually if one desires to assess each input in isolation. The minimal dispersion of the SHAP values suggests limited interaction among the variables. Consequently, the function closely resembles an additive function, a characteristic that may not be readily apparent solely from examining the equation. The plot shows the presence of two dominant variables (i.e., R_{b1} and R_{b2}), followed by R_f

Table 5 Input variables and the range for the six-variable OTL circuit function.

Range	Input variables
$R_{b1} \in [50, 150]$	Resistance b1 [K-Ohms]
$R_{b2} \in [25, 70]$	Resistance b2 [K-Ohms]
$R_f \in [0.5, 3]$	Resistance f [K-Ohms]
$R_{c1} \in [1.2, 2.5]$	Resistance c1 [K-Ohms]
$R_{c2} \in [0.25, 1.2]$	Resistance c2 [K-Ohms]
$\beta \in [50, 300]$	Current gain [Amperes]

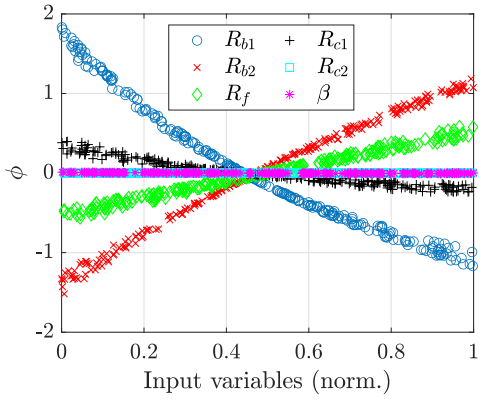

Fig. 10 Combined SHAP dependence plots for the six-dimensional OTL circuit function extracted from the PCE model

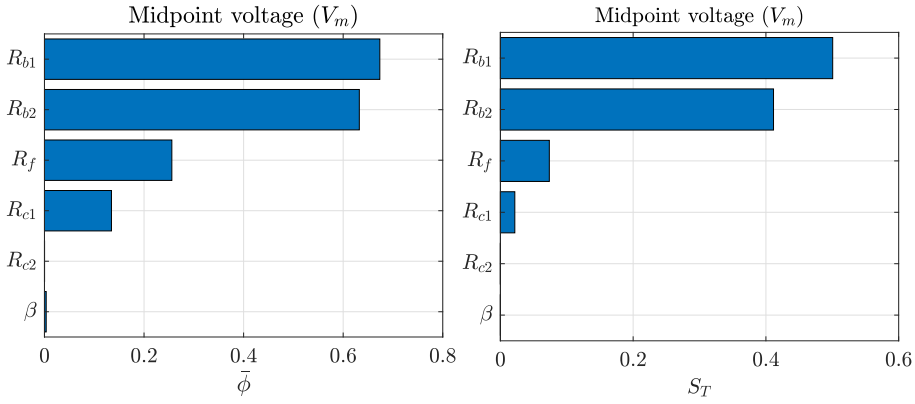

(a) Averaged SHAP **(b) Total Sobol indices**

Fig. 11 Averaged SHAP and Sobol indices computed from the PCE model applied on the six-dimensional OTL circuit function.

and R_{c1}. On the other hand, the plot also shows that the impact of R_{c2} and β is insignificant and can be neglected for practical purposes. The correlation between the input variables and V_m can also be clearly seen. The change in R_{b1} and R_{c1} negatively correlates with V_m (by keeping other variables fixed). Put differently, if R_{b1} and R_{c1} decrease, it would result in an increase in V_m. The slight nonlinearity due to R_{b1} and R_{b2} can also be observed from the figure.

Conversely, increasing R_f and R_{b2} would lead to increased V_m (i.e., positive correlation). It is important to note that there is a positive correlation between R_{c2} and V_m, whereas the correlation between R_{c1} and V_m is nearly negligible. The averaged SHAP and the Sobol indices, are depicted in Fig. 11. Both GSA metrics agree in terms of the importance ranking of the input variables.

B. Results for individual SHAP dependence plots

Figures 12, 13, and 14 show the individual SHAP dependence plots for L/D, OEW, and fuel burn, respectively. Please note that the scales are adjusted based on the minimum and maximum of the single-variable SHAP values to ensure the trends are visible. The input variables are shown in their original units.

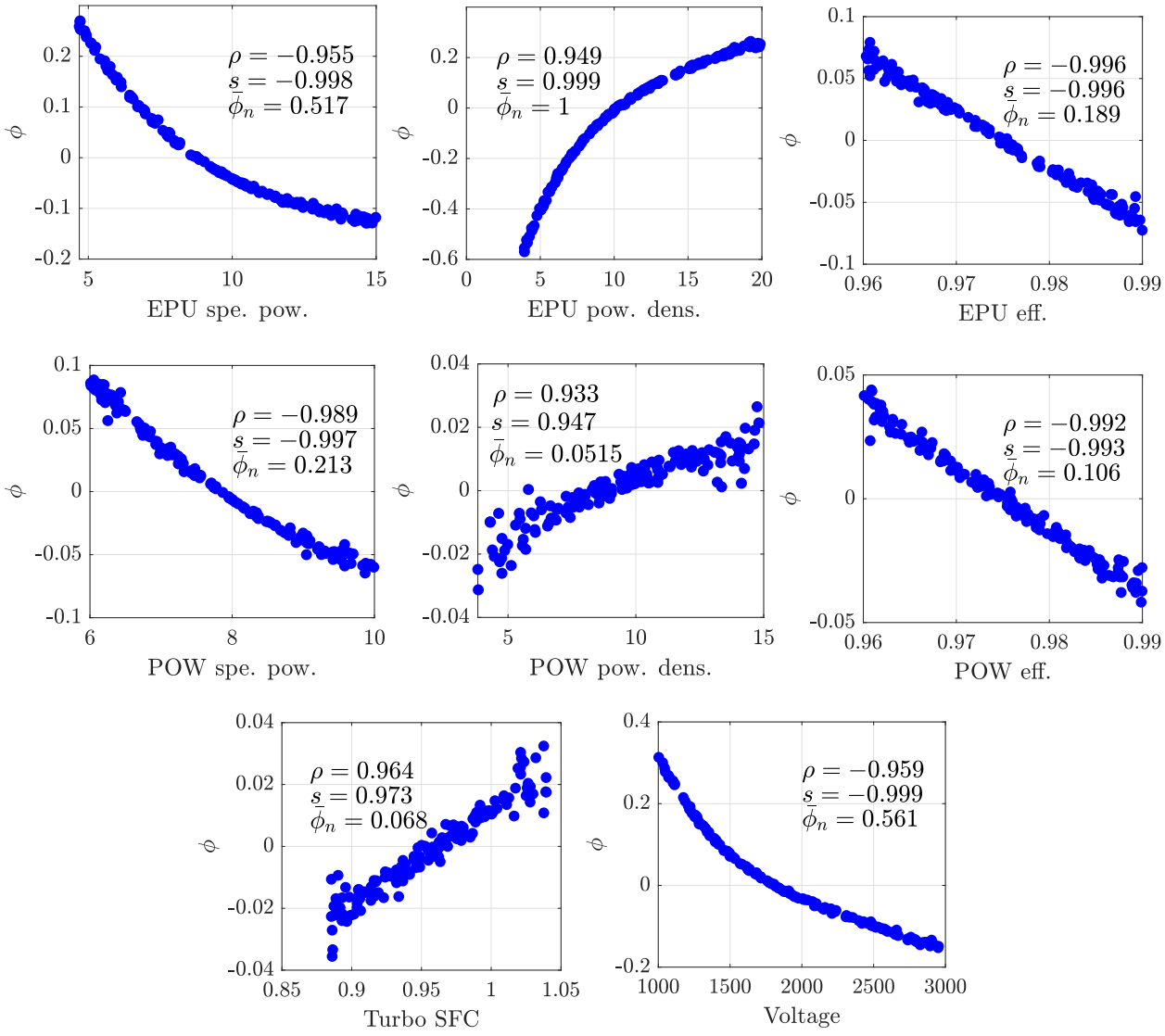

Fig. 12 Single-variable SHAP dependence plots for L/D extracted from the PCE model.

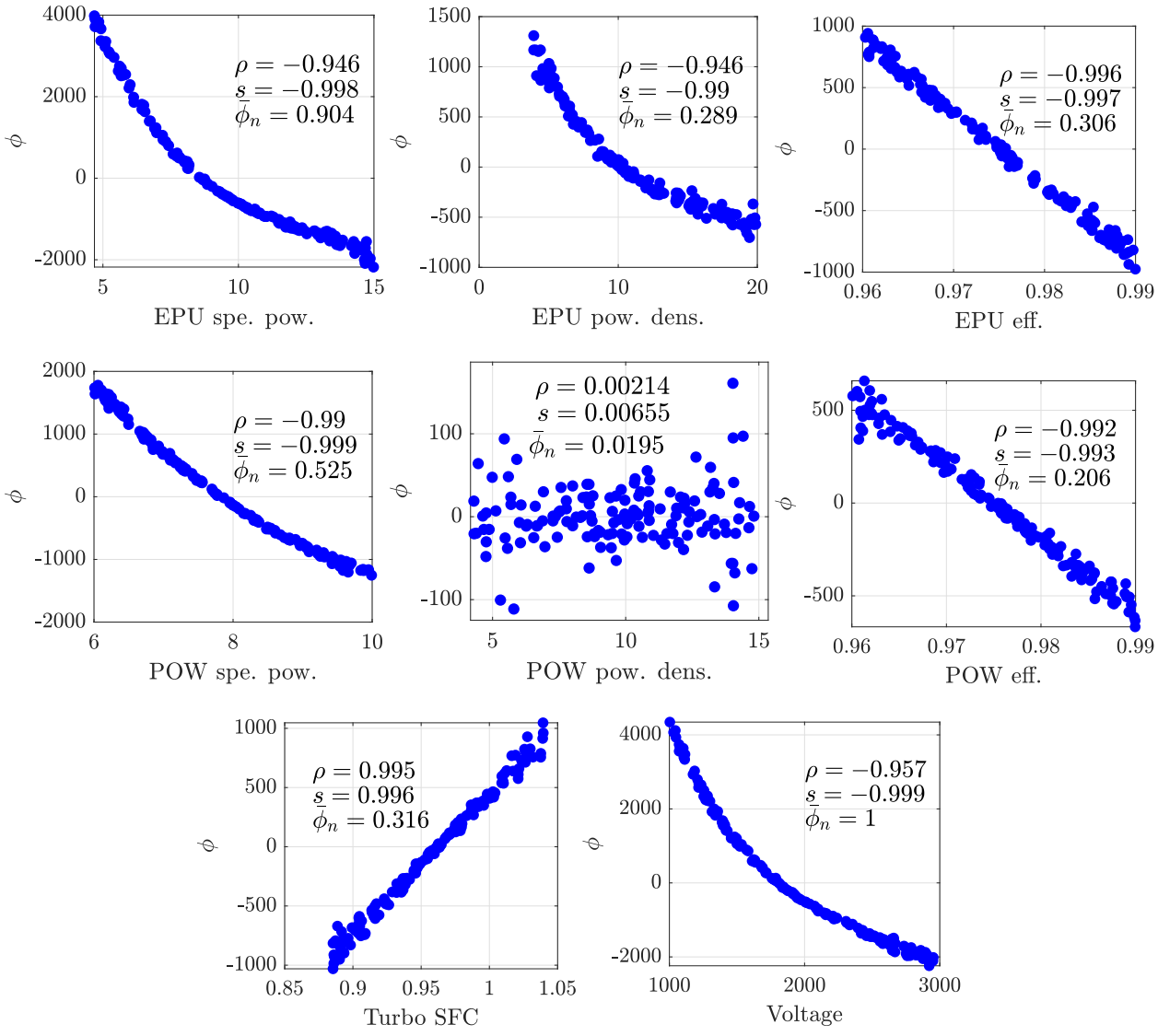

Fig. 13 Single-variable SHAP dependence plots for OEW extracted from the PCE model.

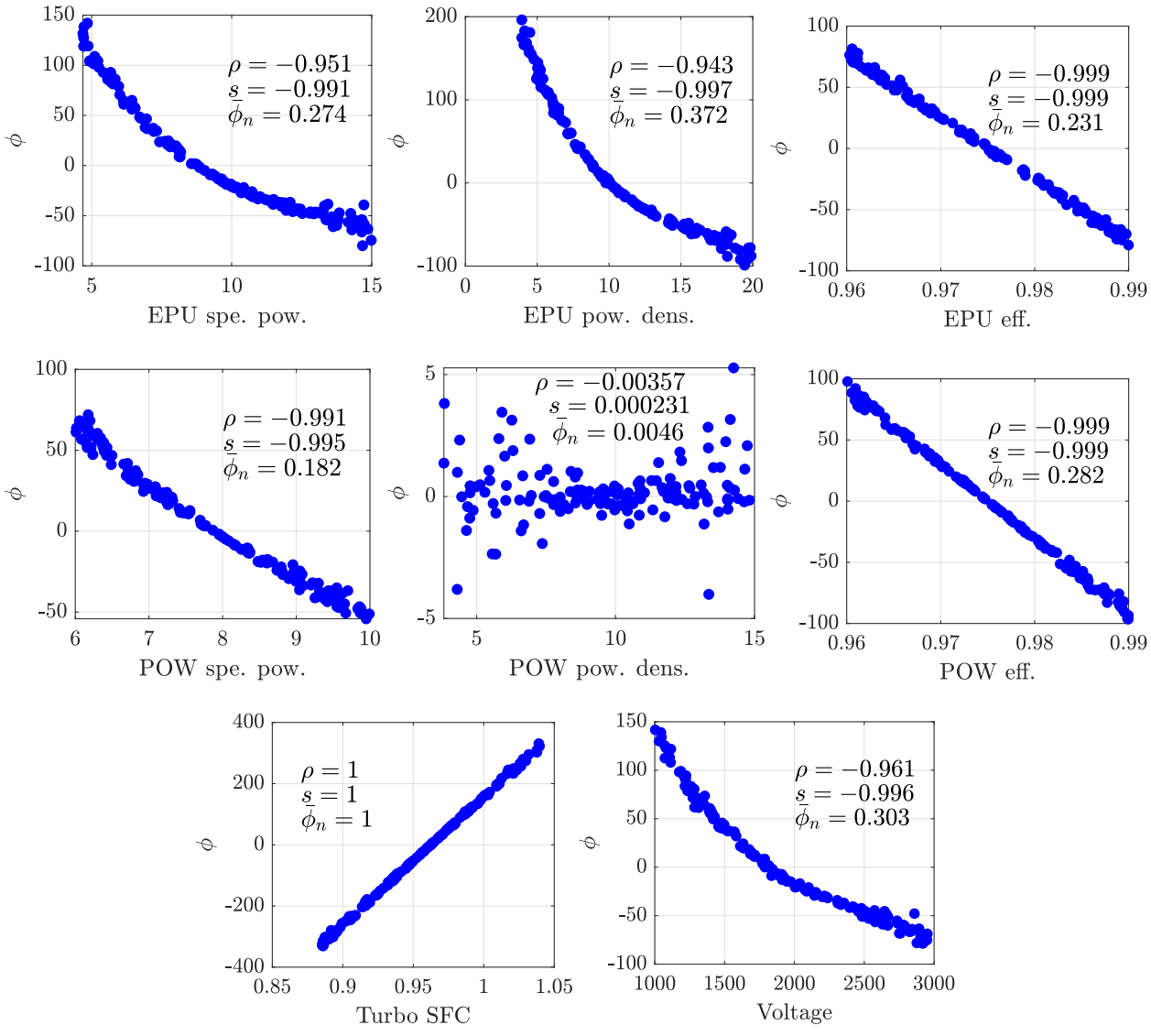

Fig. 14 Single-variable SHAP dependence plots for the fuel burn extracted from the PCE model.

References

[1] Felder, J., Kim, H., and Brown, G., "Turboelectric distributed propulsion engine cycle analysis for hybrid-wing-body aircraft," *47th AIAA aerospace sciences meeting including the new horizons forum and aerospace exposition*, 2009, p. 1132. https://doi.org/https://doi.org/10.2514/6.2009-1132.

[2] Liu, C., Doulgeris, G., Laskaridis, P., and Singh, R., "Thermal cycle analysis of turboelectric distributed propulsion system with boundary layer ingestion," *Aerospace Science and Technology*, Vol. 27, No. 1, 2013, pp. 163–170. https://doi.org/https://doi.org/10.1016/j.ast.2012.08.003.

[3] Samuelsson, S., and Grönstedt, T., "Performance analysis of turbo-electric propulsion system with fuselage boundary layer ingestion," *Aerospace Science and Technology*, Vol. 109, 2021, p. 106412. https://doi.org/https://doi.org/10.1016/j.ast.2020.106412.

[4] Jansen, R., Kiris, C. C., Chau, T., Machado, L. M., Duensing, J. C., Mirhashemi, A., Chapman, J., French, B. D., Miller, L., Litt, J. S., Denham, C., Lynde, M., Campbell, R., Hiller, B., and Heersema, N., "Subsonic single aft engine (SUSAN) transport aircraft concept and trade space exploration," *AIAA Scitech 2022 Forum*, 2022, p. 2179. https://doi.org/https://doi.org/10.2514/6.2022-2179.

[5] Schiltgen, B. T., and Freeman, J., "ECO-150-300 design and performance: a tube-and-wing distributed electric propulsion airliner," *AIAA Scitech 2019 Forum*, 2019, p. 1808. https://doi.org/https://doi.org/10.2514/6.2019-1808.

[6] Sgueglia, A., Schmollgruber, P., Bartoli, N., Atinault, O., Benard, E., and Morlier, J., "Exploration and sizing of a large passenger aircraft with distributed ducted electric fans," *2018 AIAA Aerospace Sciences Meeting*, 2018, p. 1745. https://doi.org/https://doi.org/10.2514/6.2018-1745.

[7] Saves, P., Bartoli, N., Diouane, Y., Lefebvre, T., Morlier, J., David, C., Nguyen Van, E., and Defoort, S., "Bayesian optimization for mixed variables using an adaptive dimension reduction process: applications to aircraft design," *AIAA SCITECH 2022 Forum*, 2022, p. 0082. https://doi.org/https://doi.org/10.2514/6.2022-0082.

[8] Roscher, R., Bohn, B., Duarte, M. F., and Garcke, J., "Explainable machine learning for scientific insights and discoveries," *IEEE Access*, Vol. 8, 2020, pp. 42200–42216. https://doi.org/10.1109/ACCESS.2020.2976199.

[9] Palar, P. S., Dwianto, Y. B., Zuhal, L. R., Morlier, J., Shimoyama, K., and Obayashi, S., "Multi-objective design space exploration using explainable surrogate models," *Structural and Multidisciplinary Optimization*, Vol. 67, No. 3, 2024, pp. 1–24. https://doi.org/https://doi.org/10.1007/s00158-024-03769-z.

[10] Blatman, G., and Sudret, B., "Adaptive sparse polynomial chaos expansion based on least angle regression," *Journal of computational Physics*, Vol. 230, No. 6, 2011, pp. 2345–2367. https://doi.org/https://doi.org/10.1016/j.jcp.2010.12.021.

[11] Lundberg, S. M., and Lee, S.-I., "A unified approach to interpreting model predictions," *Advances in neural information processing systems*, Vol. 30, 2017. https://doi.org/https://doi.org/10.48550/arXiv.1705.07874.

[12] Friedman, J. H., "Greedy function approximation: a gradient boosting machine," *Annals of statistics*, 2001, pp. 1189–1232. https://doi.org/10.1214/aos/1013203451.

[13] Goldstein, A., Kapelner, A., Bleich, J., and Pitkin, E., "Peeking inside the black box: Visualizing statistical learning with plots of individual conditional expectation," *journal of Computational and Graphical Statistics*, Vol. 24, No. 1, 2015, pp. 44–65. https://doi.org/https://doi.org/10.1080/10618600.2014.907095.

[14] Ribeiro, M. T., Singh, S., and Guestrin, C., ""Why should I trust you?" Explaining the predictions of any classifier," *Proceedings of the 22nd ACM SIGKDD international conference on knowledge discovery and data mining*, 2016, pp. 1135–1144. https://doi.org/https://doi.org/10.1145/2939672.2939778.

[15] Štrumbelj, E., and Kononenko, I., "Explaining prediction models and individual predictions with feature contributions," *Knowledge and information systems*, Vol. 41, 2014, pp. 647–665. https://doi.org/https://doi.org/10.1007/s10115-013-0679-x.

[16] Palar, P. S., Zuhal, L. R., and Shimoyama, K., "Enhancing the explainability of regression-based polynomial chaos expansion by Shapley additive explanations," *Reliability Engineering & System Safety*, Vol. 232, 2023, p. 109045. https://doi.org/https://doi.org/10.1016/j.ress.2022.109045.

[17] Shen, Y., Huang, W., Yan, L., Wang, Z.-g., and Xu, D.-f., "An automatic visible explainer of geometric knowledge for aeroshape design optimization based on SHAP," *Aerospace Science and Technology*, Vol. 131, 2022, p. 107993. https://doi.org/https://doi.org/10.1016/j.ast.2022.107993.

[18] Zhao, J., Wang, B., Lyu, Q., Xie, W., Guo, Z., and Wang, B., "Compression after multiple impact strength of composite laminates prediction method based on machine learning approach," *Aerospace Science and Technology*, Vol. 136, 2023, p. 108243. https://doi.org/https://doi.org/10.1016/j.ast.2023.108243.

[19] He, X., Tan, J., Rigas, G., and Vahdati, M., "On the explainability of machine-learning-assisted turbulence modeling for transonic flows," *International Journal of Heat and Fluid Flow*, Vol. 97, 2022, p. 109038. https://doi.org/https://doi.org/10.1016/j.ijheatfluidflow.2022.109038.

[20] Wu, C., Wang, S., Zhang, X.-L., and He, G., "Explainability analysis of neural network-based turbulence modeling for transonic axial compressor rotor flows," *Aerospace Science and Technology*, 2023, p. 108542. https://doi.org/https://doi.org/10.1016/j.ast.2023.108542.

[21] Sobol, I. M., "Global sensitivity indices for nonlinear mathematical models and their Monte Carlo estimates," *Mathematics and computers in simulation*, Vol. 55, No. 1-3, 2001, pp. 271–280. https://doi.org/https://doi.org/10.1016/S0378-4754(00)00270-6.

[22] Sudret, B., "Global sensitivity analysis using polynomial chaos expansions," *Reliability Engineering & System Safety*, Vol. 93, No. 7, 2008, pp. 964–979. https://doi.org/https://doi.org/10.1016/j.ress.2007.04.002.

[23] Schmollgruber, P., Atinault, O., Cafarelli, I., Döll, C., François, C., Hermetz, J., Liaboeuf, R., Paluch, B., and Ridel, M., "Multidisciplinary exploration of DRAGON: an ONERA hybrid electric distributed propulsion concept," *AIAA Scitech 2019 Forum*, 2019, p. 1585. https://doi.org/10.2514/6.2019-1585.

[24] Schmollgruber, P., Donjat, D., Ridel, M., Cafarelli, I., Atinault, O., François, C., and Paluch, B., "Multidisciplinary Design and performance of the ONERA Hybrid Electric Distributed Propulsion concept (DRAGON)," *AIAA Scitech 2020 Forum*, American Institute of Aeronautics and Astronautics, 2020. https://doi.org/10.2514/6.2020-0501, URL https://arc.aiaa.org/doi/10.2514/6.2020-0501.

[25] Nguyen, E., Defoort, S., Ridel, M., Donjat, D., Viguier, C., Ali, M., Youssef, T., Gerada, D., and Gerada, C., "Design and performance evaluation of a full turboelectric distributed electric propulsion aircraft: Preliminary results of EU project IMOTHEP," *9th European Conference for Aeronautics and Space Sciences (EUCASS)*, 2022. https://doi.org/10.13009/EUCASS2022-6134.

[26] Epstein, A. H., "Aeropropulsion for commercial aviation in the twenty-first century and research directions needed," *AIAA journal*, Vol. 52, No. 5, 2014, pp. 901–911. https://doi.org/https://doi.org/10.2514/1.J052713.

[27] David, C., Delbecq, S., Defoort, S., Schmollgruber, P., Benard, E., and Pommier-Budinger, V., "From FAST to FAST-OAD: An open source framework for rapid Overall Aircraft Design," *IOP Conference Series: Materials Science and Engineering*, Vol. 1024, 2021, p. 012062. https://doi.org/10.1088/1757-899X/1024/1/012062.

[28] Novelli, P., "IMOTHEP* European project: an investigation of hybrid electric propulsion for commercial aircraft," *AIAA AVIATION 2023 Forum*, 2023, p. 4131. https://doi.org/10.2514/6.2023-4131.

[29] Mezani, S., Belguerras, W., Takorabet, N., and Lubin, T., "Sizing Electrical Machines Using OpenOffice Calc," 2022, p. 8 pages. https://doi.org/10.13009/EUCASS2022-6110, URL https://www.eucass.eu/doi/EUCASS2022-6110.pdf.

[30] McKay, M. D., Beckman, R. J., and Conover, W. J., "A comparison of three methods for selecting values of input variables in the analysis of output from a computer code," *Technometrics*, Vol. 42, No. 1, 2000, pp. 55–61. https://doi.org/https://doi.org/10.1080/00401706.2000.10485979.

[31] Xiu, D., and Karniadakis, G. E., "The Wiener–Askey polynomial chaos for stochastic differential equations," *SIAM journal on scientific computing*, Vol. 24, No. 2, 2002, pp. 619–644. https://doi.org/https://doi.org/10.1137/S10648275013878.

[32] Efron, B., Hastie, T., Johnstone, I., and Tibshirani, R., "Least angle regression," *The Annals of Statistics*, Vol. 32, No. 2, 2004, pp. 407–451. https://doi.org/10.1214/009053604000000067.

[33] Marelli, S., and Sudret, B., "UQLab: A framework for uncertainty quantification in Matlab," *Vulnerability, uncertainty, and risk: quantification, mitigation, and management*, 2014, pp. 2554–2563. https://doi.org/https://doi.org/10.1061/9780784413609.257.

[34] Ben-Ari, E. N., and Steinberg, D. M., "Modeling data from computer experiments: an empirical comparison of kriging with MARS and projection pursuit regression," *Quality Engineering*, Vol. 19, No. 4, 2007, pp. 327–338. https://doi.org/https://doi.org/10.1080/08982110701580930.